FLUID MECHANICS

The turbulent cascade in five dimensions

José I. Cardesa,* Alberto Vela-Martín, Javier Jiménez

To the naked eye, turbulent flows exhibit whirls of many different sizes. To each size, or scale, corresponds a fraction of the total energy resulting from a cascade in five dimensions: scale, time, and three-dimensional space. Understanding this process is critical to strategies for modeling geophysical and industrial flows. By tracking the flow regions containing energy in different scales, we have detected the statistical predominance of a cross-scale link whereby fluid lumps of energy at scale Δ appear within lumps of scale 2Δ and die within those of scale $\Delta/2$. Our approach uncovers the energy cascade in a simple water-like fluid, offering insights for turbulence models while paving the way for similar analyses in conducting fluids, quantum fluids, and plasmas.

Perhaps no other area of physics research has borne the influence of a rhyming verse more than turbulence, where Richardson's "Big whirls have little whirls that feed on their velocity, and little whirls have lesser whirls and so on to viscosity" (*1*) is embedded in the seminal theory of Kolmogorov, Onsager, von Weizsäcker, and Heisenberg (*2*–*5*). The last three physicists transcribed the phenomenology in terms of wave numbers, which were to become the predominant tool in theoretical studies of the energy cascade (*6*–*10*). Consequently, scale and wave number became almost interchangeable concepts. A crucial point in the development of theories was the scale locality of the cascade, understood in terms of how close wave numbers are when energy is exchanged between them (*11*). Since the advent of computer simulations, the locality of these wave number interactions has been controversial, with studies claiming evidence in favor of (*12*) or against (*13*) it. Rigorous explanations proposed for these discrepancies (*14*, *15*) advocate for the classic scale-local view of the cascade. The debate, however, has turned predominantly around the equivalence between wave number and scale, ruling out any possibility of attributing the ongoing cascade to specific whirls visible where the flow actually evolves: the real space. Furthermore, computer simulations of industrial and atmospheric flows are carried out on numerical grids representing physical space and rely heavily on the modeling of the interaction between the resolved (large) and subgrid (small) scales (*16*).

Studies of the interscale energy transfer based on real-space quantities share one of two limitations. They either focus on a subset of the source or sink terms responsible for the changes in energy at a point (*17*, *18*), or they make no use of time, thus precluding any dynamical information or knowledge of causality (*19*–*23*). Often both limitations are combined. A noteworthy exception found a delay in the peak of the correlation between energy at two different scales when following the larger-scale flow (*24*), suggesting that eddy structures transfer their energy to smaller scales. In the wake of that study, we aimed to follow individual eddy structures. This has become possible with modern data-storage facilities where flow simulations are preserved in a movie-like manner. Such data sets have enabled the verification of phenomenological descriptions that eventually feed into dynamical models.

We analyzed data from a direct numerical simulation of turbulence in a triply periodic cube, obtained by solving the Navier-Stokes equations for an incompressible fluid by means of a deterministically forced and statistically steady pseudo-spectral code (*25*). An important length scale in turbulent flows, η, is given by $\eta = \nu^{3/4}/\varepsilon^{1/4}$, where ν is the kinematic viscosity and ε is the mean rate of kinetic energy dissipation. This small-scale length is associated with the tiniest whirls of turbulence. Our $(2\pi)^3$ computational domain spanned $(1516\eta)^3$ in space and lasted 2090 small-scale time units $\tau = \sqrt{\nu/\varepsilon}$. Expressed in terms of large-scale length and time units L_{int} and T_{int} (*25*), respectively, the simulation spanned $(5.3L_{\mathrm{int}})^3$ and $66T_{\mathrm{int}}$, with snapshots stored every 0.078τ. Although previous simulations have surpassed our Reynolds number $L_{\mathrm{int}}/\eta = 284$, our long yet temporally resolved data set with a sizeable scale separation allowed us to statistically characterize a phenomenon by tracking many flow regions throughout their life.

The tracked flow regions that we now introduce in detail underpin our definition of whirls or eddies. We isolated a range of scales by filtering the velocity fields with a spatial band-pass filter. Owing to the homogeneity of the flow, we used an isotropic filter to simplify the concept of scale to a single scalar Δ. We set the center of the filter band at the chosen scale Δ and used bands of constant width on a logarithmic scale (*15*). The upper and lower edges of the band resulted from subtracting two low-pass Gaussian filters (*25*). We focused on four scales from the geometric sequence $\Delta/\eta = (30, 60, 120, 240)$. This led to four time series of the dynamics of the flow, one for each scale. The object of our study was a scalar quantity, the kinetic energy, which evolved in time t, scale Δ, and three-dimensional space (x, y, z). The kinetic energy at a scale is half the sum of the squared filtered velocity components. The flow structures in Fig. 1 are geometrically connected regions of space where the energy is above a given threshold [movie S1 (*25*)]. We chose the threshold systematically in the same way for all scales on the basis of the percolation properties of the energy at that scale (*25*, *26*). We further time-tracked these flow objects by using a technique developed for the tracking of coherent structures in turbulent channel flows (*27*). Whereas generally an object was born small as the underlying energy exceeded the threshold and died small as its intensity decreased, an object often merged

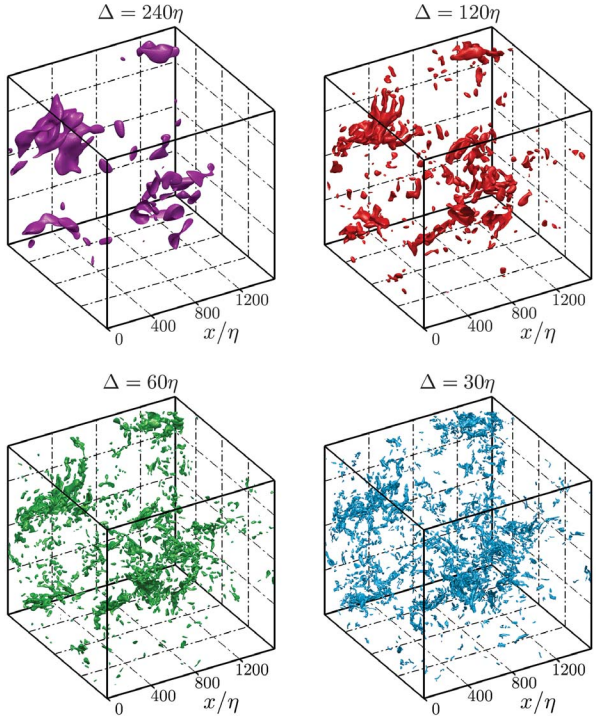

Fig. 1. Energy-eddies at four different scales Δ for the same instant in a numerical simulation of turbulence in a periodic cube. A time sequence is shown in movie S1 (*25*). The flow structures observed are the spatially connected regions of the flow where the energy at scale Δ is above a certain threshold (*25*).

School of Aeronautics, Universidad Politécnica de Madrid, 28040 Madrid, Spain.
*Corresponding author. Email: ji.cardesa@upm.es

with or split from other objects during its life. We grouped objects related by a connection at some point in space-time within the same temporal graph (*27*). We called a graph emerging from this grouping an energy-eddy, or simply eddy, because it was educed according to the intense kinetic energy that it traced. We defined the scale of the eddy as the center Δ of the filter band that we used to compute it, the volume (V) as the sum of volumes of all objects of a graph existing at a given instant, and the lifetime (T_{life}) as the time elapsed between the birth and death of the first and last object within the graph, respectively.

The volume distributions collapsed onto a single curve over a fairly wide range (Fig. 2A) with scaling parameter Δ, after neglecting the tails. The lifetime distributions scaled with the local eddy turnover time $T_{eto} = \Delta^{2/3}\varepsilon^{-1/3}$ (Fig. 2B), found by assuming that for a range of scales where $L_{int} \gg \Delta \gg \eta$, the only relevant parameters are ε and Δ (*2*). The collapse of the probability density functions (Fig. 2B) supports that T_{eto} is indeed a scaling parameter over a range of lifetimes, excepting the short-lived small-scale eddies for which viscosity cannot be neglected. A log-normal distribution resulted from a nonlinear fit to all our data (Fig. 2B), where the mean and standard deviation were the fitting parameters minimizing the difference. The parameters were 0.8 and 1.3, respectively, so that the average eddy lifetime is of the order of T_{eto}. Overall, the picture that emerges lends support to the eddy definition based on the observed scaling properties of the eddy sizes and lifetimes.

Our four time sequences provide the space-time position of the eddies at four scales. By superposing contemporary fields from any two scales at a time, we linked those two scales by computing their intersection in space. We defined the intersection ratio for a single eddy of scale A intersecting N eddies of scale B at a given instant

$$R(A,B) \equiv \frac{\sum_{i=1}^{i=N} V_i(A \cap B)}{V(A)}$$

where $V(A)$ is the volume of the eddy of scale A, and $V_i(A \cap B)$ is the intersection volume between the eddy of scale A and the ith intersected eddy of scale B (Fig. 3). This ratio is unity if the eddy of scale A is fully contained within one or more eddies of scale B, whereas it vanishes when $N = 0$ in the case of no intersections. We thus quantified how the field of scale-B eddies filled up individual eddies of scale A, which we followed.

We considered whether the intersections depended on the scale and on the stage in the life of the eddies. We split the lifetime of each scale-A eddy into equal fractions, or life stages. We then computed the mean intersection ratio $R_m(A, B)$ conditioned to a given life stage (*25*). We normalized the result by the corresponding null hypothesis (Fig. 4A), which showed intersection levels higher than random for those scale combinations separated by a factor of 2 (orange and blue curves). The intersections between eddies of scales further apart did not show a trend that was distinctly different from the null hypothesis, indicating little or no spatial overlap. We then normalized the scale combinations separated by a factor of 2 with their corresponding maximum (Fig. 4B), which revealed that curves based on combinations where $A = 2B$ peaked toward the death of the scale-A eddies, whereas with $A = B/2$, the peak was closer to their birth. This statistical signature shows unequivocally how the eddies of a given scale originate from eddies of twice their scale, whereas they give rise to eddies half their scale before disappearing. This

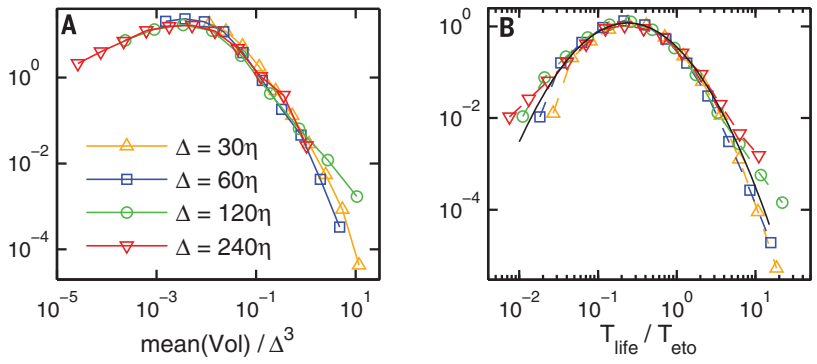

Fig. 2. Mean volumes and lifetimes of the eddies. Probability density functions of (**A**) the mean volumes and (**B**) the lifetimes of the eddies. The solid black line in (B) follows a log-normal distribution with a mean of 0.8 and a standard deviation of 1.3. The volumes used for (A) are the average over each eddy's lifetime.

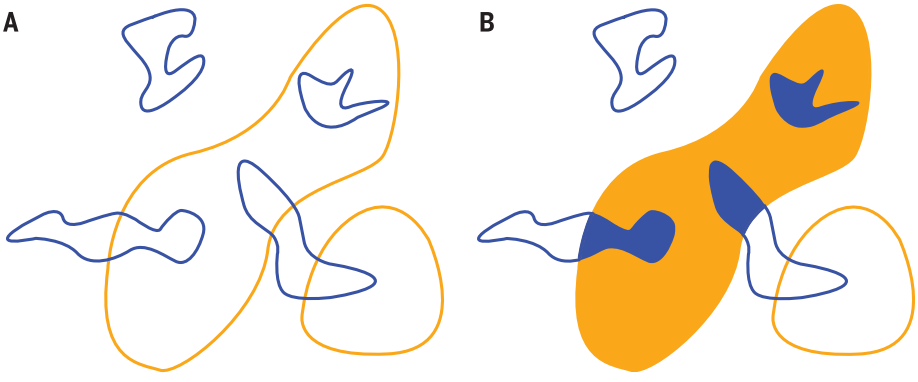

Fig. 3. Sketch illustrating the intersection ratio between eddies of scale *A* (orange) and *B* (blue). (**A** and **B**) $R(A, B)$ for the largest of the two eddies of scale A in (A) is given by the sum of the blue areas in (B), divided by the union of the blue and orange areas in (B).

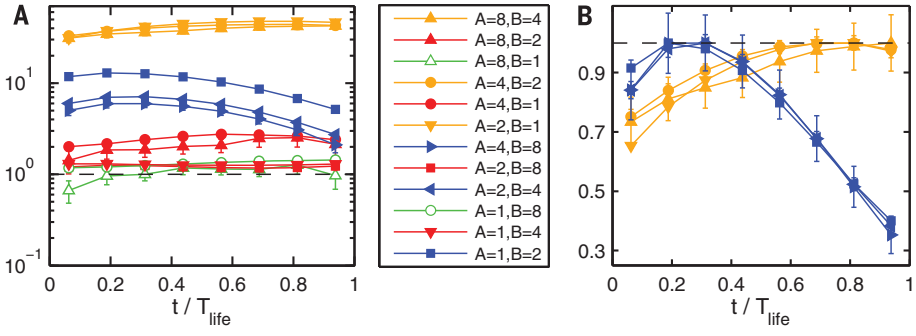

Fig. 4. Mean intersection ratio $R_m(A, B)$ between scales *A* and *B* at different stages of the life-time of scale-*A* eddies. Scales (1, 2, 4, 8) in the legend correspond to Δ/η = (30, 60, 120, 240), respectively. (**A**) Normalized by the mean intersection level obtained by randomly locating fields B with respect to A (null hypothesis) (*25*). Unity implies a random intersection level. (**B**) Same as (A) but normalized by the maximum, keeping only A and B combinations separated by a factor of 2. Error bars in (A) and (B) represent 95% confidence intervals (*31*).

process replicated itself through four successive scales, each separated by a factor of 2, which suggests that a scale-local progression of the energy from the large to the small scales is, at the very least, a transited cascade path in homogeneous three-dimensional turbulence.

The results show that energy is transferred to the smaller scales overall. This average trend is often labeled as a forward, or direct, cascade. Some individual eddies, however, follow opposite paths. To illustrate this point, we used a crude definition of a forward cascade event as an individual eddy of scale A for which $R(A, B)$ averaged over the first half of T_{life} is larger than $R(A, B)$ averaged over the second half of T_{life}, taking $A = B/2$. This occurred twice as often as backscatter events, defined as eddies for which $R(A, B)$ was larger during the second half of T_{life}, where $A = B/2$. Even though this way of quantifying the predominance of forward cascade versus backscatter is somewhat simplistic, it is important to keep such event counts in mind because the trends that we observed (Fig. 4) should not obscure the underlying bidirectionality. Large-eddy simulations, which are extensively used in engineering and meteorological contexts, require particular attention to the direction of the energy flux between the resolved and subgrid scales (*16*).

Our analysis illustrated the locality of the energy exchanges and, more broadly, the phenomenology of the turbulent cascade. We looked for and verified this statistically in physical space with individual eddies of scales separated by factors of 2, 4, and 8. Future work could include studying the interaction between eddies separated by a factor of 3 or 1.5, together with a simulation at larger scale separations where the smallest scale is outside the viscous regime. Moreover, our approach has led to an observation and not to the identification of the physical process causing it. We can now, however, design a study targeting those regions in space-time where the energy cascade takes place to understand the causes. Lastly, our method was applied to a simple flow, but nothing prevents its use in more complicated cases with additional nonlinear terms. The presence of rotation, compressibility, conductivity, and quantum effects complicates the energy cascade considerably, leading to areas of turbulence research where Richardson's verse is a more limited part of the story. Our approach could yield advances in those fields, particularly as the required data become available through numerical simulations (*28*–*30*).

REFERENCES AND NOTES

1. L. F. Richardson, *Weather Prediction by Numerical Process* (Cambridge Univ. Press, 1922).
2. A. N. Kolmogorov, *Dokl. Akad. Nauk S.S.S.R.* **30**, 299–301 (1941).
3. L. Onsager, *Nuovo Cim.* **6**, 279–287 (1949).
4. C. F. Weizsäcker, *Z. Phys.* **124**, 614–627 (1948).
5. W. Heisenberg, *Z. Phys.* **124**, 628–657 (1948).
6. A. M. Obukhov, *Dokl. Akad. Nauk S.S.S.R.* **32**, 22–24 (1941).
7. R. H. Kraichnan, *J. Fluid Mech.* **5**, 497–543 (1959).
8. C. E. Leith, *Phys. Fluids* **10**, 1409–1416 (1967).
9. I. Proudman, W. H. Reid, *Philos. Trans. R. Soc. London A* **247**, 163–189 (1954).
10. T. Tatsumi, *Proc. R. Soc. London Ser. A* **239**, 16–45 (1957).
11. R. H. Kraichnan, *J. Fluid Mech.* **47**, 525–535 (1971).
12. J. A. Domaradzki, W. Liu, M. E. Brachet, *Phys. Fluids* **5**, 1747–1759 (1993).
13. P. K. Yeung, J. G. Brasseur, *Phys. Fluids* **3**, 884–897 (1991).
14. G. L. Eyink, H. Aluie, *Phys. Fluids* **21**, 115107 (2009).
15. H. Aluie, G. L. Eyink, *Phys. Fluids* **21**, 115108 (2009).
16. P. Sagaut, *Large Eddy Simulation for Incompressible Flows: An Introduction* (Springer Science+Business Media, 2006).
17. M. Wan, Z. Xiao, C. Meneveau, G. L. Eyink, S. Chen, *Phys. Fluids* **22**, 061702 (2010).
18. J. I. Cardesa, A. Vela-Martín, S. Dong, J. Jiménez, *Phys. Fluids* **27**, 111702 (2015).
19. T. Aoyama *et al.*, *J. Phys. Soc. Jpn.* **74**, 3202–3212 (2005).
20. U. Piomelli, W. H. Cabot, P. Moin, S. Lee, *Phys. Fluids* **3**, 1766–1771 (1991).
21. S. Cerutti, C. Meneveau, *Phys. Fluids* **10**, 928–937 (1998).
22. P. A. Davidson, B. R. Pearson, *Phys. Rev. Lett.* **95**, 214501 (2005).
23. R. J. Hill, *J. Fluid Mech.* **468**, 317–326 (2002).
24. C. Meneveau, T. S. Lund, *Phys. Fluids* **6**, 2820–2825 (1994).
25. Materials and methods, along with a movie, are available as supplementary materials.
26. F. Moisy, J. Jiménez, *J. Fluid Mech.* **513**, 111–133 (2004).
27. A. Lozano-Durán, J. Jiménez, *J. Fluid Mech.* **759**, 432–471 (2014).
28. J. C. Perez, J. Mason, S. Boldyrev, F. Cattaneo, *Phys. Rev. X* **2**, 041005 (2012).
29. N. Navon, A. L. Gaunt, R. P. Smith, Z. Hadzibabic, *Nature* **539**, 72–75 (2016).
30. M. Wan *et al.*, *Phys. Plasmas* **23**, 042307 (2016).
31. L. H. Benedict, R. D. Gould, *Exp. Fluids* **22**, 129–136 (1996).

ACKNOWLEDGMENTS

We thank A. Lozano-Durán for providing the code for the tracking of flow structures. All authors acknowledge funding from project COTURB (Coherent Structures in Wall-bounded Turbulence) of the European Research Council. The data for this study were obtained using the DECI-PRACE (Distributed European Computing Initiative–Partnership for Advanced Computing in Europe) resource Minotauro, based in Spain at the Barcelona Supercomputing Centre. M. P. Encinar helped with making the data public. The flow fields are freely available from our online database at https://torroja.dmt.upm.es/turbdata/Isotropic.

SUPPLEMENTARY MATERIALS

www.sciencemag.org/content/357/6353/782/suppl/DC1
Materials and Methods
Figs. S1 to S6
Table S1
References (*32*, *33*)
Movie S1

19 May 2017; accepted 26 July 2017
Published online 17 August 2017
10.1126/science.aan7933

Science

The turbulent cascade in five dimensions

José I. Cardesa, Alberto Vela-Martín and Javier Jiménez

Science **357** (6353), 782-784.
DOI: 10.1126/science.aan7933originally published online August 17, 2017

Tackling the life and death of whirls

Energy in a turbulent system moves from large eddies to smaller ones until it is dissipated by viscous motion. The details of exactly how this works have remained obscure, in part because of the challenge of simulating fluids across many length scales in three dimensions over time. Cardesa *et al.* present a large numeric simulation of a water-like fluid that shows characteristic length scales for the birth and death of turbulent whirls. The approach can be extended to understand energy transfer in the atmosphere, plasmas, and other complex systems.

Science, this issue p. 782